一种基于视觉的平面焊缝初始焊位定位的简易方法

陈希章[1,2], 陈善本[2], 林 涛[2]
(1. 江苏大学 材料科学与工程学院, 江苏 镇江 212013;
2. 上海交通大学 焊接工程研究所, 上海 200030)

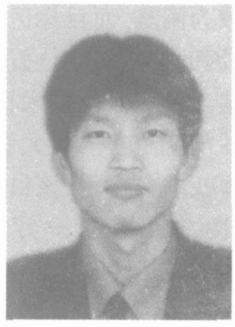
陈希章

摘 要: 焊缝起始位置的自动定位是实现智能化焊接的关键步骤之一。介绍了一种实用的视觉引导焊接机器人到初始焊位的导引系统和方法。在系统中, 机器人可以在视觉系统的引导下自动定位到任意平面焊缝的起始位置。以铝这种强反射平面曲线对接焊缝工件为例, 实现了初始焊位的自主定位功能。系统具有算法简单, 实用性和稳定性以及抗干扰性强等特点, 其定位准确率和精度都在试验中取得了满意的结果。

关键词: 视觉; 定位; 初始焊位; 弧焊机器人
中图分类号: TG403 文献标识码: A 文章编号: 0253-360X(2006)03-73-04

0 序 言

将机器人应用于焊接领域大大提高了焊接自动化水平, 彻底改变了以往焊接过程刚性自动化的传统方式, 开拓了一种柔性的自动化生产方式[1,2]。传统示教再现焊接机器人对焊接作业条件的稳定性及精度要求十分严格, 不具备自主获取工件定位信息和焊缝空间位置信息的能力, 无法适应现在的小批量多品种的生产模式。焊接机器人具有一定的自主能力具有十分重要的现实意义。就机器人焊接作业而言, 焊接机器人运动轨迹控制主要指初始焊位导引与焊缝跟踪控制技术[2,3]。当焊接机器人在完成某项焊接任务时, 对于任何任务都需要使焊枪准确移动到初始焊接位置, 并且调整焊枪的姿态使之满足焊接工艺的要求。将焊接机器人导引到初始焊接位置的过程是实现焊接机器人自主焊接的关键步骤之一。

目前, 对于无初始位置信息的初始焊接位置的寻找、识别以及对焊接机器人导引方面的研究很少。有的生产企业和机器人公司在极小的范围有接触式的焊接始端检出和导引, 但只是盲点的接触传感, 远非自主, 适用范围很小, 不具备对焊接环境变化的自主视觉识别与导引功能。

机器视觉技术的发展以及性能可靠、体积小、价格低的 CCD传感器的出现使得视觉成为自动控制中常用的一种传感方法。文献[4,5]应用立体视觉技术初步探讨了焊接机器人的初始焊位导引问题, 但复杂的算法及立体视觉中的标定、立体匹配等环节加大了定位误差, 影响了定位结果的稳定性, 运算速度慢且误差较大, 达不到实时焊接的引弧要求。而在实际焊接工程中, 很大一部分焊件是平面焊缝(包括直线曲线等各种接头), 因此探讨一种针对这种焊缝的简单实用且稳定的初始焊位定位方法具有很大的现实意义。

收稿日期: 2004-12-17
基金项目: 上海市科委重点攻关项目(02111111116)

1 初始焊位在图像上位置的确定

要想利用摄像机检测到焊缝起点位置, 就要知道它在弧焊机器人基坐标系中的坐标, 以控制机器人运动到要求的目标点。第一步就是要检测出焊缝起点在工件图像上的位置。这涉及到图像识别和边缘提取等图像处理技术。由于物理世界的复杂性和各种噪声的引入, 使得被处理的图像信号相当复杂, 目标的识别变得不易实现。图像处理技术已经发展了许多年, 至今仍不完善, 处于不断改进和发展中。研究人员在各种算法上做了大量的工作, 但没有一种通用的技术对各种各样的图像都能得到令人满意的结果, 甚至也没有一个理论来指导选择特定方法处理特定图像。焊接环境较为复杂, 如焊件表面的不一致性(划痕、氧化色、标记、油污等等), 又如弧光的干扰。图 1为对接铝板待焊工件的照片, 可以看到有明显的灰度不均匀现象, 同时边缘上有很强的反光, 且反光的位置和强度会随着工件位置的摆放和工作车间的光源变换而有不同, 光照强烈时, 焊枪、送丝嘴等甚至在工件上形成倒影, 具有“镜面”效应。同时工作台、夹具等所形成的焊接工作环

境使得焊缝的识别异常困难。这使得通过搜索焊缝形成的边缘求取特征点的识别方法[4,5]变得很难实现。因此必须针对焊接环境的特点对进行焊缝的识别和特征的提取。

1.1 模板匹配原理

根据前面的分析，对整个焊接环境进行识别和定位较为困难，而目标区域仅仅是初始的焊接位置而已，因此仅对初始位置区域进行识别是一条可行的办法。模板匹配技术恰恰在这方面体现出优势。模板匹配就是在一幅大图像中搜寻目标，已知该图中有要找的目标，且该目标同模板有相同的尺寸、方向和图像，通过一定的算法可以在图中找到目标，确定其坐标位置。这样就可以避免对这个焊接环境进行识别求取焊缝的边缘。为了衡量模板与待匹配图像某区域的匹配程度，对于数字图像，可用式(1)来表示模板与对应图像之间的相似度[5,6]。

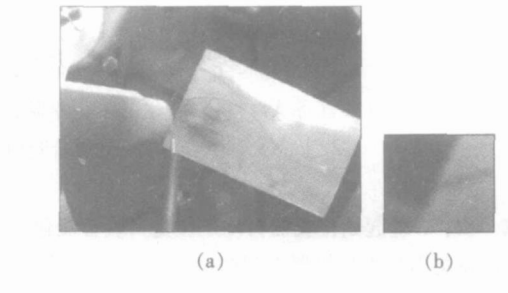

图 1 原始焊接图像及其模板

Fig. 1 Origin image and its template

$$R(i,j)=\frac{\sum_{x=0}^{L-1}\sum_{y=0}^{K-1}[w(x,y)-\bar{w}][f(x+i,y+j)-\bar{f}(i,j)]}{\left[\sum_{x=0}^{L-1}\sum_{y=0}^{K-1}[w(x,y)-\bar{w}]^2\right]^{\frac{1}{2}}\left\{\sum_{x=0}^{L-1}\sum_{y=0}^{K-1}[f(x+i,y+j)-\bar{f}(i,j)]^2\right\}^{\frac{1}{2}}},\tag{1}$$

式中：f为待匹配图像；w为模板图像；R为在待匹配的大图像中模板图像所覆盖区域。$i=0,1,2,\cdots,M-1$；$j=0,1,2,\cdots,N-1$；$\bar{w}$是w的平均值；而$\bar{f}(x,y)$是$f(x,y)$与w当前位置相对应区域的平均值。相关系数$R(i,j)$通过归一化尺度变换到区间$[-1,1]$中，所以其值与$f(x,y)$和$w(x,y)$的幅度值变化无关，可用来衡量模板匹配的相似程度。

1.2 标准模板的制取

焊接初始点的定位实际上是在焊接作业前进行的工作，所以在没有焊接的条件下直接从原图像中提取模板，见图 1右侧的小图像。在得到一幅模板以后，将此模板叠加到实时拍摄的焊接图像上进行匹配，比较模板和模板覆盖下的焊缝图像的相关程度，相关性越大，说明子图与模板的匹配程度越好。最后选取匹配程度最好的子图像作为匹配输出。这样就可以根据此模板准确的匹配出该区域的位置。但是工作环境的光线等条件可能随时间变化，同时工件的装夹位置等也在变化，图像帧与帧间感兴趣的目标就有所变化，这样仍用这个模板进行匹配就会使得结果不准确。但总的来讲，图像目标区域总体结构信息是不变的，这就需要根据焊接工作环境的特点，通过人的先验知识选取一幅最有代表性的且包含同一类型焊缝普遍特征的模板作为匹配模板。也可根据 8邻域像素的灰度差值特点制作人工模板。

1.3 目标点的像素细分

采用上述模板匹配法可以确定一个像素的定位误差，为了获得更高的像素定位精度，可以通过多项式插值获得高准确度的边缘位置。

目标点的坐标可近似为图 2中的像元几何中心(x_c,y_c)。这时其准确度受 CCD 光敏元间距W、H的约束，W为像元x方向的间距，H为像元y方向间距。为了进一步提高准确度，采用多项式插值边缘算法，其表达式[7]为

$$y(x)=\sum_{k=0}^{n}l_k^{(n)}(x)f(k),\tag{2}$$

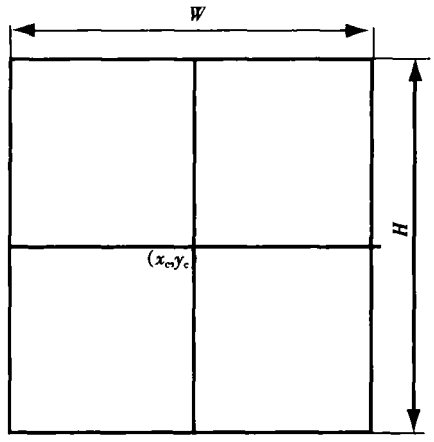

图 2 得到的像元位置

Fig. 2 Coordinates of pixel

$$l_k^{(n)}(x)=\frac{(x-x_0)\cdots(x-x_{kx-1})(x-x_{k+1})\cdots(x-x_n)}{(x_k-x_0)\cdots(x_k-x_{k-1})(x_k-x_{k+1})\cdots(x_k-x_n)},\tag{3}$$

式中: $y(x)$为插值函数; $l_k^{(n)}(x)$为插值基函数; $f(k)$为函数值; x_k 为插值基点。对于目标点 (x_c, y_c), 其梯度图像 $f(i,j)$分别在 x、y 方向上取三点 $f(i-1,j)$、$f(i,j)$、$f(i+1,j)$和 $f(i,j-1)$、$f(i,j)$、$f(i,j+1)$为函数值, x_i-W、x_i、x_i+W和 y_j-H、y_j、y_j+H为插值点, 分别代入式(3), 可分别求得 x、y 方向的二次插值函数, 令该函数的微分为零, 可求得目标点的坐标 (x_g, y_g)为

$$x_g = x_c + \frac{f(i-1,j) - f(i+1,j)}{f(i-1,j) - 2f(i,j) + f(i+1,j)} \cdot \frac{W}{2}, \tag{4}$$

$$y_g = y_c + \frac{f(i,j-1) - f(i,j+1)}{f(i,j-1) - 2f(i,j) + f(i,j+1)} \cdot \frac{H}{2}。 \tag{5}$$

2　机器人系统定标

物体识别和定位都是在像素坐标系中进行的, 得到的图像上物体的位置和方向都是以像素坐标系为基准的。但对于实际的应用, 人们关心的是物体的实际场景坐标, 对于机器人系统就是机器人的参考坐标系。这需要通过标定来解决问题。在视觉系统中, 摄像机的标定在很大程度上决定了最后计算结果的精度。而目前通用的技术中无论是传统的标定方法还是自标定方法都要建立复杂的模型和计算方法。定位精度较高的标定方法需要采用试验室用的昂贵测量仪器。这就大大限制了该方法在工业生产中的实际应用。针对焊接生产中多数工件是平面焊接件的情况, 采用计算机视觉技术, 应用简易可靠的平面标定方法, 避免使用精确度高但价格非常昂贵的试验室专用设备, 使得该方法具有较高的工业实用性。

如图 3所示, O_p-$x_p y_p$ 为图像平面坐标系, 依据图像在计算机中的存储顺序, 原点在图像左上角, 单位是像素。O_i-$X_i Y_i$ 为工件坐标系统, 单位是 mm, O_r-$X_r Y_r Z_r$ 为机器人参考坐标系。

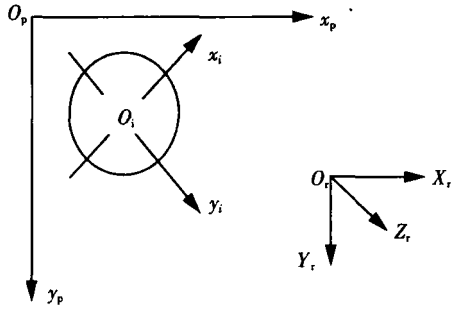

图 3　标定坐标系

Fig. 3　Coordinates system

由图像上的像素点坐标求取参考坐标系对应点的坐标问题, 可以分为两步完成, 首先确定像素坐标和工件坐标系之间对应点的坐标变换关系, 然后再确定工件坐标系和机器人参考坐标系之间的变换关系。

在两个二维坐标系中, 点的坐标变换是简单的线性变换关系, 即

$$P = \boldsymbol{R}_p + \boldsymbol{T}, \tag{6}$$

式中: $\boldsymbol{R}$ 是二维旋转变换矩阵; $\boldsymbol{T}$ 是二维平移矩阵。用矩阵形式表示就是

$$\begin{bmatrix} X \\ Y \end{bmatrix} = \begin{bmatrix} \boldsymbol{R}_{00} & \boldsymbol{R}_{01} \\ \boldsymbol{R}_{10} & \boldsymbol{R}_{11} \end{bmatrix} \begin{bmatrix} x \\ y \end{bmatrix} + \boldsymbol{T}。 \tag{7}$$

将一个单位圆固定在工件坐标系中, 圆心对应于工件坐标系的坐标原点。这样可以知道多个特征点在工件坐标系和机器人坐标系中的坐标, 同时通过图像处理可以知道它的图像坐标, 因此联立方程可以求得旋转和平移矩阵。

$$\begin{bmatrix} X_i \\ Y_i \end{bmatrix} = \begin{bmatrix} 0.2073 & -0.1007 \\ -0.1126 & -0.2310 \end{bmatrix} \begin{bmatrix} x_p \\ y_p \end{bmatrix} + \begin{bmatrix} -22.4941 \\ 56.9254 \end{bmatrix}。$$

$$\begin{bmatrix} X_r \\ Y_r \end{bmatrix} = \begin{bmatrix} 0.50 & 0.9 \\ 0.9306 & -0.4532 \end{bmatrix} \begin{bmatrix} X_i \\ Y_i \end{bmatrix} + \begin{bmatrix} 1064.3 \\ 26.5930 \end{bmatrix}。$$

这样通过 CCD拍摄工件图像, 通过上述算法找出目标点的图像坐标通过上面两个公式代入可以求得目标点在机器人坐标系中的坐标, 从而控制机器人运动到目标点进行焊接。

3　试　　验

试验在自行开发的智能焊接机器人系统 WR-SR7的试验平台上展开, 试验中采用的摄像机镜头为 WAT902H, CCD靶面尺寸为 1/2英寸, 取像像素为 768×576。采用为大恒 CG-400图像采集卡完成图像的采集。

图 4给出了试验的流程图, 将焊接机器人导引到焊接初始位置以后, 误差范围在允许范围内时, 可以直接起弧焊接, 如果在一些误差较大的情况下, 要进行局部的纠偏运算, 因为较大的误差一般由于在抓取图像时焊枪或者送丝嘴等遮挡住了焊接位置而使得计算不准确, 这样等定位到大体位置后, 再次在较低位置取像, 进行再次运算就可以达到满意的结果。

图 5给出了 X、Y 方向的定位误差, 其中评价的标准是以示教所得初始焊接位置的坐标值作为真实值, 以计算的定位坐标与示教结果相比较得出误差值。总共试验 18次, 即将工件在工作台上随机移动, 得出结果。从图中可以看出 X、Y 方向误差大部

分在 3 mm以内, 但是可以看到, 第 7、8次试验结果误差较大, 误差绝对值在 5 ~ 6 5之间, 明显不能满足直接起弧焊接的要求。引起这个误差的原因是在取像位置, 送丝嘴或者焊枪等遮挡住了焊接的起始位置, 图 6给出了一种遮挡情况的图片, 这样在图像处理时就不能得到准确的初始点位置, 从而导致大的误差。这就要用图 4所示的流程图中的误差纠正的办法进行纠偏以达到工艺要求。经过大量的试验, 排除遮挡情况, 以示教测量的位置坐标值为真值, 一次定位误差在 3 mm 以内的成功率在 96%以上, 如果加上二次纠偏功能, 在有限次试验内定位成功率达 100%。 3 mm 的误差可以达到对初始焊位粗定位的目的, 方便下一步的纠偏。同时还应注意如果反光点恰好落在目标点, 对定位精度也有一定影响, 其中图 5的第 14次试验结果就属于这种情况, 误差达到 3. 9mm。而钢等对光线不如此敏感的材料可以更为准确的定位到焊接初始位置。

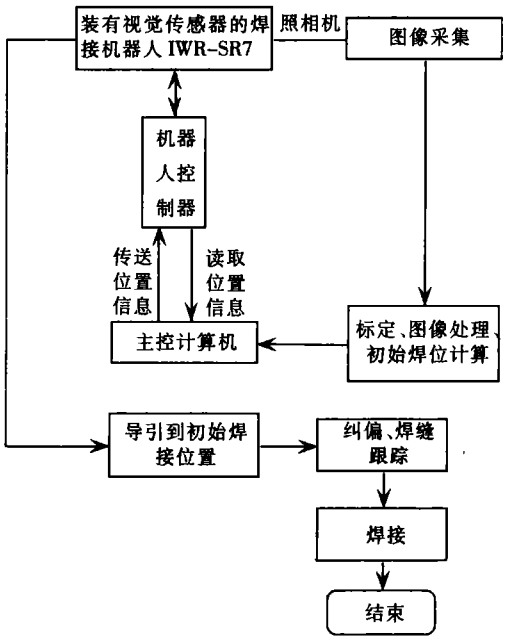

图 4 工作流程图

Fig. 4 Flow chart of localization

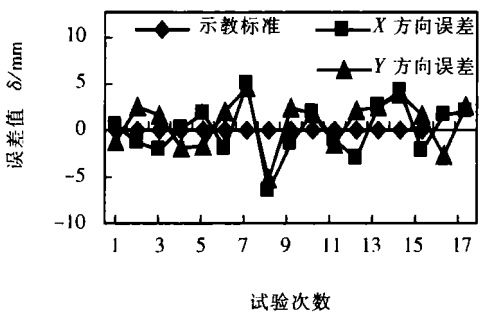

图 5 定位误差

Fig. 5 Error of localization

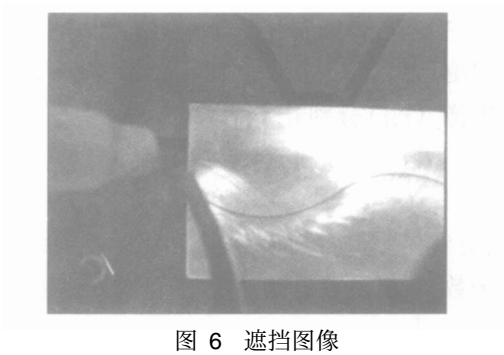

图 6 遮挡图像

Fig. 6 Image sheltered from torch or wire feeder setting

4 结 论

采用模板匹配和平面标定方法, 成功地实现了真实焊接环境下平面焊缝初始焊位的视觉定位, 方法简单, 定位精度和准确度高。对实际焊接工程中大量的平面焊件具有很强的适应性, 但对有遮挡的情况定位误差较大, 可以通过二次纠偏的方法加以解决。与生产企业的接触寻找定位方法相比, 该方法具有更大的适应性, 提高了焊接智能化的水平。而与立体视觉方法相比, 则省略了复杂的立体标定和困难的立体匹配计算, 提高了定位精度。该方法是一种简单实用且具有一定智能水平的初始焊位定位方法, 具有较高的使用价值。

参考文献:

[1] 潘际銮. 二十一世纪焊接可许研究的展望[A]. 第九次全国焊接会议论文集[C]. 哈尔滨: 黑龙江人民出版社, 1999. 1 - 7.

[2] Tam T J, Chen S B, Zhou C J. Robotic welding: intelligent and automatio[M]. Springer Verlag, Mar. 2004.

[3] 陈善本, 吴 林. 焊接智能化技术现状与发展[A]. 第十次全国焊接会议论文集[C]. 哈尔滨: 黑龙江人民出版社, 2001. 84 - 96.

[4] 李金泉. 基于视觉的弧焊机器人焊缝空间位置信息获取技术的研究[D]. 哈尔滨: 哈尔滨工业大学, 2003.

[5] 朱振友, 朴永杰, 林 涛, 等. 基于视觉的局部环境焊缝起始位置识别方法[J]. 焊接学报, 2004, 25(2): 95 - 99.

[6] Gonzalez R C. Digital image processing: second edition[M]. 北京: 电子工业出版社, 2002.

[7] 徐翠薇. 计算方法引导论[M]. 北京: 高等教育出版社, 2001.

作者简介: 陈希章, 男, 1976年 10月出生, 讲师, 博士研究生。研究方向为焊接机器人智能化及焊接过程自动化, 发表论文 10篇。

Email: xzhchen@sjtu.edu.cn

D/A converter, and the output parameters of welding can be easily controlled with high precision. At the same time, the welding device has lower complexity. Moreover, the welding parameters can be regulated contemporary and output current of variable polarity pulsed welding can be exactly controlled.

Key words: digital signal processing; variable polarity; pulsed metal inert gas

Identification of aluminum alloy pulsed metal inert gas welding dynamic process SHI Yu, HUANG An, FAN Ding, LIANG Wei-dong (State Key Lab of Gansu Non-ferrous Metal Materials, Lanzhou University of Technology, Lanzhou 730050, China). p57 - 60

Abstract: Based on the step response experiment, the welding pool width model of dynamic process in aluminum alloy pulsed metal inert gas welding was identified by least square method. The input of the model was welding wire speed and base current respectively, and the output was beam width of welding pool. The influence of wire speed and base current on welding pool width was analyzed. It provides the theoretical basis to realize the intelligent control for aluminum alloy pulsed metal inert gas welding process.

Key words: aluminum alloy; pulsed metal inert gas welding; identification

Metallic ceramic arc spraying cored wires for surface modification of cranshaft GUO Mian-huan, LIU Ai-guo, ZHAO Min-hai, Qu Jun-zhang (1. National Key Laboratory of Advanced Welding Production Technology, Harbin Institute of Technology, Harbin 150001, China). p61 - 64

Abstract: Cored wires with Al_2O_3 and NiCr-Cr_3C_2 as filler materials for surface modification of cranshaft were produced. Microstructures, bonding strength and wear-resistance of coatings produced with these two cored wires were tested. The results showed that with Al_2O_3 as filler material of the cored wire, content of ceramic phase in the coating was high, and the coating was fairly bonded to the substrate. Adhesive strength was as high as 21.23 MPa, and the shear strength of the coating was 31.27 MPa. Resistance to wear of the coating was good. With same wear conditions, the wear loss of mass was only one-fourth of that of the cast iron sample. Addition of Ni_3Al and graghite was the most important reason for high adhesive strength.

Key words: cored wire; cranshaft; thermal spray; metallic ceramic

Environmental load assessment of arc welding process BU Zhi-xiang, SHI Yu-xiang, WANG Bin, PENG Zhi-fang (College of Power & Mechanical Engineering, Wuhan University, Wuhan 430072, China). p65 - 68

Abstract: By introducing LCA (life cycle assessment) environmental assessment method to arc welding process, it is presented that the involved material quantity of power, resource and waste per unit volume or mass of welding deposited metal (welding product) can be defined as a technical parameter for environmental load assessment of welding process, which provides a new method to quantitatively investigate environmental load of welding. The results from the environmental load assessment of CO_2 gas shielded arc welding indicate that waste is the key factor which should be controlled and improved to affect the product making environment. The assessment model has been proved reasonable from the fact that power factorial item of CO_2 gas shielded arc welding shows good comparability with correlative item of steel-making process in electric oven, which makes it possible to quantitatively assess the whole life cycle of materials.

Key words: life cycle assessment; arc welding; CO_2 gas shielded arc welding; environmental load; panenvironment function

Solidification characteristics and mechanism of feeding surface metallurgical coating by DC-plasma jet LI Min[1,2], LI Hui-dong[1,2], LI Hui-qi[1,2], PEI Zhong-an[2], SUN Yu-zong[2] (1. Institute of Material, Beijing University of Science and Technology, Beijing 100083, China; 2. Institute of Material, Shandong University of Science and Technology, Qingdao 266510, Shandong, China). p69 - 72

Abstract: The ferroalloy coatings with powder mixtures of different constituent, different size, different density and different shape were prepared on Q235 steel using the feeding surface metallurgical technology by DC-Plasma Jet. The composition, microstructure of alloying coating and microstructure transformation of heat-affected zone were investigated using optical microscope, scanning electron microscope, electron microprobe analysis and X-ray diffraction. Results indicated that plasma surface metallurgical coating of Fe-Cr-Ni-B-Si had well wettability and metallurgical bonding was obtained between coating and substrate. The rapid solidifing structure of coating was laminar from epitaxial planar crystal on the bottom to equiax crystal in the middle to bunchy crystal on the top. The matrix of surface coating was malleable γ-(Fe, Ni) dendritic cyrstal which was supersaturated solid solution of many Cr and small Ni, B, Si, C elements. And eutectic structure of $(Cr, Fe)_7(C, B)_3$ and γ-(Fe, Ni) dispersed on interdendrite. Due to heat cycle influenced by plasma beam, the heat-affected zone had two layers: phase transformation zone and recrystallization zone.

Key words: plasma surface metallurgy; solidification characteristics; ferroalloy powder

A simple method to locate initial welding position of planar weld using visual technology CHEN Xi-Zhang[1], CHEN Shan-ben[2], LIN

Tao[2] (1. School of material science and engineering, Jiangsu University, Zhenjiang 212013, Jiangsu, China; 2. Institute of Welding Engineering, Shanghai Jiao tong University, Shanghai 200030, China). p73 – 76

Abstract: The autonomous localization of initial welding position of weld is one of the key technologies to realize the intellectualized welding. This paper presented a practical system and method to guide the welding robot to the initial welding position of weld. In this system, welding robot can be guided to the initial welding position of any planar weld automatically by the aid of a charge coupled device camera. Aluminium and its alloy can reflect the light strongly, which make the recognition more difficult. Taking butt joint weld of planar curve aluminium sheet as examples, the autonomous localization function is realized accurately. This method is simple, practical, jarless and strong anti-jamming. And experimental results show that it has higher accuracy rate and precision, and it can meet the requirements of production.

Keywords: vision; localization; initial weld position; arc welding robot

Cu-Ti composite diffusion coating for joining Si_3N_4 ceramic to metal

ZHANG Hong-xia, WANG Wen-xian, ZHOU Cui-lan, MENG Qing-sen (College of Material Science and Engineering, Taiyuan University of Technology, Taiyuan 030024, China). p77 – 80, 85

Abstract: A method of multiple ion compounds diffusion coating alloy (MICDCA) technology was put forward. The alloy layer was directly deposited on the Si_3N_4 ceramic surface by MICDCA method, and brazing of Cu-Ti alloying ceramic to metal was realized with MICDCA. The diffusion coating was tested by energy dispersive spectrometer, X-ray diffractometer, scanning electron microscope, optical microscope and anchoring strength scratching test. It was indicated that diffusion coating consist of Cu, Ti, Fe, Si and Al element, and Cu and Ti distributed uniformly. The diffusion coating was made up of Cu_2Ti, Cu, $TiSi_2$, and anchoring strength of deposited and substrate was well under the maximum of 100 N, the diffusion coating did not stripped and avalanched from the ceramic substrate. Si_3N_4 ceramic with diffusion coating was joined to metal, and the joining was analyzed using 100 times optical microscope and 5 000 times scanning electron microscope. It was indicated that joining strength was well and there were not obvious macroscopic and microcosmic defects. The method was carried out in a comparatively low vacuum and provided a new method for joining ceramic to metal.

Keywords: Si_3N_4 ceramic; Cu-Ti composite diffusion coating; surface alloyed; brazing

Melting characteristic of twin electrode single arc welding I: Heating and melting of twin electrode

HAN Bin[1], ZOU Zeng-da[2], QU Shi-yao[2] (1. School of Mechanical and Electronic Engineering, Petroleum University, dongying 257061, Shandong, China; 2. School of Materials Science and Engineering, Shandong University, Jinan 250061, China). p81 – 85

Abstract: With measuring dynamic temperature change of twin electrode, the heating and melting of twin electrode single arc welding was investigated. Results show that the melting coefficient of twin electrode increases with increasing of welding current, decreasing of coating weight coefficient and decreasing of two-core span, and it is 2 – 3 times than that of single core electrode. During twin electrode single arc welding, the energy used for heating and melting twin electrode includes resistance heat in core rod and arc heat. The melting of the electrode mainly depends on the arc heat. When the electrode was closely used up, for the current of 200 A, the increase in temperature of TE4303 electrode was approximately 750 ℃. TE308-16 electrode had high temperature evolution and fast melting rate. The range of temperature field generated by the arc heat in an electrode is generally within 16mm from the electrode end.

Keywords: twin electrode; single arc welding; heating and melting; electrical resistance heat; arc heat

Mechanism of high strength and high toughness of HSLA weld deposited metal

Yang Jun, Wu Lu-hai, Mao Ji-fang (School of Materials Science and Technology, Shanghai Jiaotong University, Shanghai, China, 200030). p86 – 90

Astract: It was effective to resist precipitation of grain boundary ferrite and make fine homogeneous acicular ferrite formation by transferring suitable amount of Ti-B elements and suitable amount of rare earth elements so that it increased low temperature toughness of weld deposited metal. It had been found that weld alloy elements could be the nucleating centers of acicular ferrite as long as they formed fine non-metallic inclusions which were difficult to dissolve by the investigation of transmitted electron microscope. Titanium could form such fine combination nucleus (TiO) which spreaded in the weld metal and was acicular ferrite nucleus forming. Acicular ferrite consisted of a lot of substructure, and it was the microstructural reason to improve the low temperature toughness of weld deposited metal.

Keywords: weld; acicular ferrite; low temperature toughness; high strength low alloy steel

Crack tip stress field and fracture parameter of welded joints with cracks located at fusion line under mixed loading

ZHANG Min[1], FU Chong[1], LI Ji-hong[1], ZHOU Rong-can[2], LI Yi-min[2] (1. School of Material Sierce and Engineering, Xi'an University of Technology, Xi'an 710048, China; 2. Reserd Center of Material Engineering, Xi'an Thermal Power Research Institute, Xi'an 710032, China). p91 – 95

Abstract: Concentrated on the mismatched welded joints contain defects located at its fusion line, the stress strain fields distribution was analyzed by elasto-plastic finite element method with mixed mode loading